Article

Process Intensification of Methane Production via Catalytic Hydrogenation in the Presence of Ni-CeO$_2$/Cr$_2$O$_3$ Using a Micro-Channel Reactor

Vut Tongnan [1], Youssef Ait-lahcen [2], Chuthamas Wongsartsai [1], Chalempol Khajonvittayakul [1], Nuchanart Siri-Nguan [3], Navadol Laosiripojana [4] and Unalome Wetwatana Hartley [1,4,*

[1] Chemical and Process Engineering, The Sirindhorn International Thai-German Graduate School of Engineering (TGGS), King Mongkut's University of Technology North Bangkok, Bangkok 10800, Thailand; vut.t-dcpe2018@tggs.kmutnb.ac.th (V.T.); chuthamas.w-cpe2016@tggs.kmutnb.ac.th (C.W.); chalempol.k-cpe2016@tggs.kmutnb.ac.th (C.K.)

[2] Process Engineering, National Polytechnic Institute of Chemical Engineering and Technology, 4 Allee Emile Monso, 31030 Toulouse, France; youssef.a-cpe2018@tggs.kmutnb.ac.th

[3] PTT Public Company Limited, Ayutthaya 10908, Thailand; nuchanart.s@pttplc.com

[4] Joint Graduate School of Energy and Environment (JGSEE), King Mongkut's University of Technology Thonburi, Bangkok 10140, Thailand; navadol@jgsee.kmutt.ac.th

* Correspondence: unalome.w.cpe@tggs-bangkok.org; Tel.: +66-2-555-2930

Abstract: A slight amount of Cr$_2$O$_3$ segregation in 40 wt% NiO/Ce$_{0.5}$Cr$_{0.5}$O$_2$ was presented at the surface. The best catalytic performance towards the reaction was achieved at 74% of CO$_2$ conversion and 100% CH$_4$ selectivity at 310 °C, the reactant (H$_2$/CO$_2$) feed molar ratio was 4, and the WHSV was 56,500 ml$_N$·h^{-1}·g$^{-1}_{cat}$. The mechanistic pathway was proposed through carbonates and formates as a mediator during CO$_2$ and H$_2$ interaction. Activation energy was estimated at 4.85 kJ/mol, when the orders of the reaction were ranging from 0.33 to 1.07 for nth-order, and 0.40 to 0.53 for mth-order.

Keywords: Ni-CeO$_2$/Cr$_2$O$_3$; micro-channel reactor; CO$_2$ methanation; wash-coated method; synthetic natural gas

1. Introduction

CO$_2$ is one of the greenhouse gases (GHGs), well-known for causing the climate change and global warming. This study proposes CO$_2$ conversion to methane via CO$_2$ hydrogenation or the so-called methanation process. The reaction generally occurs at moderately a high temperature ranging from 250 to 400 °C [1] associated with the reverse water gas shift (RWGS) reaction [2]. Ni-doped high porous supports were extensively studied for such a process during the past decades. Ni/SiO$_2$ prepared using metal-organic framework (MOF) derivatives were studied by Ye et al., (2021) [3]. It was reported that the nickel phyllosilicate, formed by bonding between Ni and silicate enhanced the stability of the catalyst towards the reaction. The catalyst offered 77.2% of CO$_2$ conversion and 100% CH$_4$ selectivity; at 310 °C, under 20 bar, within 52 h of reaction time (T$_{50}$ = 270 °C). Atzori et al., (2019) [4] synthesized 25% Ni/CeO$_2$–ZrO$_2$ (3:1 ratio of CeO$_2$/ZrO$_2$) using the soft-template method which was found to provide even better catalytic performance compared with the Ni/SiO$_2$. The catalyst provided 85% CO$_2$ conversion and 100% CH$_4$ selectivity at a relatively lower operating temperature of 300 °C, after running for 6 h (T$_{50}$ = 260 °C). From this study, it was suggested that CO$_2$ adsorption occurred on CeO$_2$/ZrO$_2$, whereas gaseous H$_2$ reacted with the active Ni species. The effect of Ni content and the choice of supports in the catalyst system were studied by Gac et al., (2019) [5], where the level of Ni varied from 10 to 40% by weight on various supports, i.e., CeO$_2$, ZrO$_2$, and Al$_2$O$_3$. It was reported that the optimal Ni loading was between 20 and 30% at T$_{50}$ = 250 °C, whereas the activity of the catalyst system, when using a

different support, was ordered as $Al_2O_3 < ZrO_2 < CeO_2$. The number of Ni active surfaces is basically increased by the higher Ni doping level; however, the Ni agglomeration often occurs when the Ni level is more than 30%, resulting in a drop in the number of Ni active surfaces. Nevertheless, this is not the case when using Al_2O_3 as a support due to its relatively high surface area. Despite its excellent ability to disperse Ni and its high thermal stability, Al_2O_3 as a support, offered a lower synergy effect in terms of catalytic activity of the overall catalyst system, compared with the study by Ceria-Zirconia Bukhari et al., (2019) [6] who added Ni at 1, 3, 5, and 10 wt% into fibrous SBA-15, to investigate the effect of Ni loading. The result showed that 5% Ni/fibrous SBA-15 provided the best activity amongst all with 98.9% CO_2 conversion and 99.6% CH_4 selectivity at 400 °C for 120 h. This was due to some specific characteristics of the catalyst system which include (1) homogeneous and well-dispersed Ni particles on the support, (2) strong metal-support interaction, and (3) high surface basicity. However, when the catalytic activity was found to decrease when the Ni loading was higher than 10% due to the agglomeration as explained earlier. Jaffar et al., (2019) [7] studied the effect of various parameters, i.e., temperature, gas hourly space velocity (GHSV), H_2:CO_2 ratio, choice of metals (Ni, Fe, Co, and Mo) and the type of supports (Al_2O_3, SiO_2 and MCM-41) on the methanation process via CO_2 hydrogenation. The 10% Ni/Al_2O_3 was found to provide the highest CO_2 conversion of 83% and CH_4 yield of 94% at 360 °C, amongst all the studied catalysts. The zeolitic supports, i.e., SiO_2 and MCM-41, were not reported as the most promising material due to its hydrophilicity. In this phenomena, Si-O-Si would be formed on the surface via H_2O (byproduct) adsorption, favoring water gas shift (WGS) reaction. This resulted in a decrease in CH_4 yield and an increase in CO formation. Besides, the carbonyl surface species formation (on the zeolitic supports) can be inhibited by water surface coverage. The influence of different preparation methods for NiO-CeO_2 was also studied by Cárdenas-Arenas et al. (2020) [8]. The results showed that the reversed micro-emulsion method provided the best activity in terms of CO_2 conversion (80%) and CH_4 yield (98%) at 400 °C for 25 h (T_{50} = 300 °C), due to its highest specific surface area (122 m^2/g), small crystal size (6–7 nm), and highly reducible Ni-O-Ce species on the surface. Bi-metallic catalysts have been excessively researched recently [9–11]. The effect of different types of promoters, i.e., Zr, Ce, La, and Mo, has been studied [9,10]. Although La was reported to offer sufficient catalytic activity (83% CH_4 yield at 300 °C (T_{50} = 265 °C)), due to its high basicity, allowing strong CO_2 adsorption; however, Ce was able to provide the better catalytic performance (CO_2 conversion of 76.4% and CH_4 selectivity of 99.1% at 350 °C for 10 h (T_{50} = 240 °C)). In addition, the TOF value of CeO_2 was found to be the highest amongst the selected promoters; thus, it can generate more active sites, resulting in an increase in the catalyst's intrinsic rate. The observation from many previous works reported that the activity of CO_2 methanation is generally increased with temperature; however, CH_4 selectivity would be halted once it reached a certain limit. The catalyst deactivation is observed during high temperature operation, due to the catalyst sintering. The CH_4 selectivity is usually encouraged at a relatively low operating temperature; however, the reaction occurs at a low kinetic rate, since the kinetic rate of a certain reaction can be enhanced by an optimal design of reactor. Thus, to optimize the catalytic performance of the methanation process is to maintain the high CO_2 methanation as well as the high CH_4 selectivity. Therefore, the process intensification becomes another crucial concern, rather than the sole development of the catalysts. A micro-reactor or micro-channel reactor can the enhance overall performance of a particular chemical reaction process, due to its small residence time, low mass/heat transfer limitation, narrowed product distribution and rapid responding behavior [12–14].

The micro-channel catalytic reactors were proven to increase productivity compared with other similar-sized conventional reactors [1], due to higher catalyst surface-to-volume ratios. Besides, a catalyst in a micro-channel reactor is generally applied by using a wall-coating technique. This means that there is no concerned pressure drop across the catalyst's bed, unlike in the conventional packed-bed reactor [15]. In the meantime, catalyst selection is still one of the most crucial issues for the process development. The right

catalyst increases the desired products by reducing their reaction's activation energies, while also hindering the unwanted side reactions. These actions lead to the elimination of thermodynamic limitation, and less complication in a post-reaction-separation unit due to its narrower product distribution.

The methanation catalysts generally consist of two parts: (1) transition/noble metal, i.e., Ni, Fe, Co, Ru or Pd, acts as an active site [2]; and (2) (mixed) metal oxide, i.e., Al_2O_3, SiO_2, ZrO_2, CeO_2, La_2O_3, MgO, TiO_2, carbon materials and zeolites, act as a support [12,13]. CeO_2 was chosen as a support in the present work because of its outstanding oxygen storage capacity and its ability to promote the active metal dispersion [14]. Besides, the oxygen vacancy of CeO_2 can be tailored to needs by substituting the smaller transition metal ion (compared with Ce) into it such as Zr^{4+} or Cr^{3+} [16]. The high oxygen vacancy material is well-known to improve its acidic/basic catalytic properties for CO/CO_2 adsorption capability [15,17]. Several previous studies reported that CeO_2/Cr_2O_3 established higher oxygen vacancy than CeO_2/ZrO_2 [18,19]. Vannice et al. (1977) [2] compared the activities of group VIII metals that were dispersed on Al_2O_3. The result showed that the order of the activity ranked from high to low as Ru >> Fe > Ni > Co > Rh > Pd > Pt > Ir. Although Ru is superior, its cost is high. Fe or Ni therefore received greater attention due to its reasonable price and sufficient catalytic activity. Nie et al. (2017) [20] studied Ni content by varying percentage of Ni, which was doped on $Ce_{0.9}Zr_{0.1}O_2$, from 10 to 40%. It was found that CO_2 conversion reached its maximum at 95% when Ni level was 40%. According to our previous work [21], Ni doped on $Ce_xCr_{1-x}O_2$ of which the stoichiometric ratio (x) was 0.5, is one of the superior catalyst supports for simultaneously maximizing CO_2 conversion and CH_4 selectivity. In this work, 40% Ni-CeO_2/Cr_2O_3 was prepared using the one-pot hydrolysis method. The catalyst was wash-coated inside a stainless-steel micro-channel reactor. Physicochemical properties of the catalyst were investigated using an X-ray diffractometer (XRD), hydrogen temperature-programmed reduction (H₂-TPR), and Fourier-transform infrared spectroscopy (FTIR). The effect of operating parameters on the catalytic performance was investigated. The mechanism of the gas-solid reaction and kinetics were also predicted.

2. Results and Discussion

2.1. Characterizations

2.1.1. XRD

Figure 1 compares XRD patterns between the catalyst 40% Ni-CeO_2/Cr_2O_3 (1:1) catalyst (d) and the pure NiO (a), Cr_2O_3 (b), CeO_2 (c). The catalyst diffractogram resembled the CeO_2 phase structure, identified at 28.64, 33.16, 47.61, 56.32, 59.02, and 69.45; whereas the NiO phase was found at 37.30, 43.34, and 62.92 (JCPDS No. 01-078-0429). However, no Cr_2O_3 phase (2θ at 24.57, 33.53, 36.34, 41.58, 44.60, 50.37, 54.93, 58.35, 63.20, and 65.18 with JCPDS card No. 38-1479) was detected in the catalyst's diffractogram, implying that Cr was substituted into the Ce lattice with none or little segregation of Cr to the catalyst surface. This can be due to the fact that the ionic radius of 3D transition metal is smaller than the cerium ions radius (0.615 Å for Cr^{3+} versus 1.01 Å for Ce^{4+} [16]). The CeO_2 peaks shown in the catalyst's diffractogram were slightly shifted to a higher degree, compared with the pure CeO_2 which were positioned at 28.54, 33.12, 47.34, 56.20, 58.92, and 69.30 (JCPDS card No. 03-065-5923). This was due to the substitution of a smaller Cr ion into the CeO_2 lattice, creating a larger channel radius in the lattice and high oxygen mobility [22] while the fluorite structure was remained. The NiO peak in the catalyst was seen to be broader than that in pure NiO (a), indicating that the NiO in the catalyst system has a smaller particle size, resulting in good dispersion of Ni on the CeO_2/Cr_2O_3. This result agreed with TPR results in the later section.
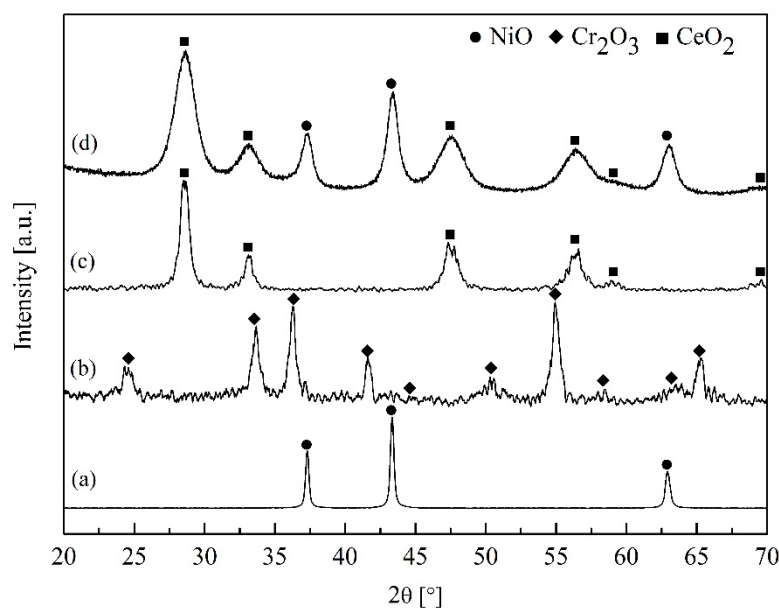
Figure 1. XRD patterns of (**a**) pure NiO (●), (**b**) Cr_2O_3 (▲), (**c**) CeO_2 (■) as an external standard for peak positions identification, and (**d**) 40 wt% Ni-CeO_2/Cr_2O_3 calcined at 500 °C.
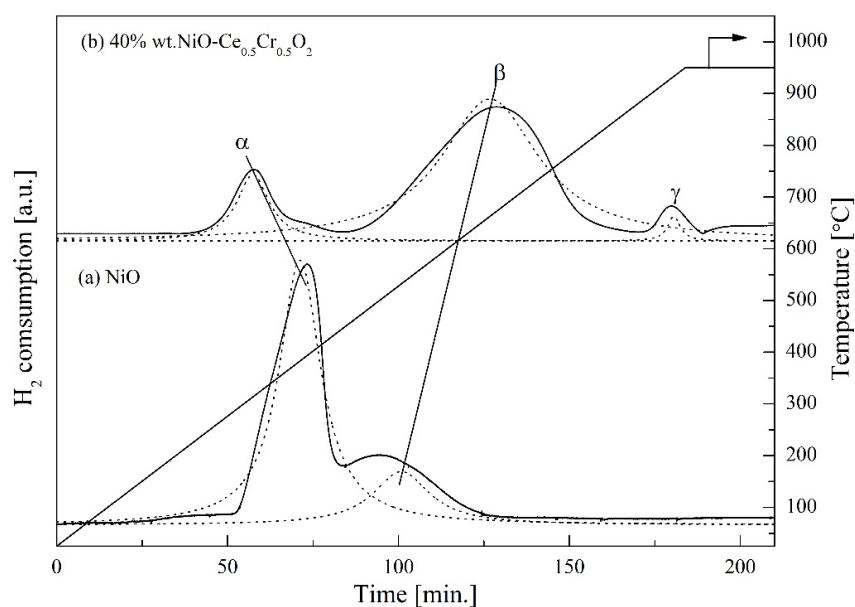
2.1.2. H_2-TPR

The catalyst reducibility was studied by the temperature programmed reduction (TPR) technique using 5% H_2/Ar. In Figure 2, it can be seen that for pure NiO (a), two distinct peaks were observed and centered at 380 °C (peak α) and 500 °C (peak β), attributing to a reduction in Ni^{2+} ions to metallic Ni at the surface and bulk oxygen, respectively. This result agreed with the work reported by other researchers [23]. The TPR spectrum of the catalyst (b) showed three reduction peaks. The first peak (peak α) was due to reduction in NiO, which occurred at 310 °C, and lower than the reduction temperature of pure NiO. This indicates good dispersion of NiO on the CeO_2/Cr_2O_3 [24], which resulted from the smaller particle size of Ni at the surface. The strong bonding interaction between NiO and the support (CeO_2/Cr_2O_3) was suggested, as the peak β of the catalyst was found at a higher temperature compared with that of pure NiO [24]. The peak γ of the catalyst was found at a temperature higher than 900 °C. This peak is the result of $NiCr_2O_4$ spinel [25] or $CeCrO_3$ perovskite [26] which were formed via NiO + Cr_2O_3 → $NiCr_2O_4$ or $2Ce_{0.5}Cr_{0.5}O_{2+\delta}$ → $CeCrO_3$ + $(0.5 + \delta)O_2$, indicating that a slight amount of Cr_2O_3 presented at the surface; however, it was not sufficient to be detected by XRD.

2.1.3. SEM Morphology before and after Catalyst Coating

The SEM images of the substrates were observed as shown in Figure 3: where Figure 3(a1) and Figure 3(a2) represent the surface before the cleansing process; Figure 3(b1) and Figure 3(b2) are for the surface after the cleansing process; and Figure 3(c1) and Figure 3(c2) demonstrate the substrate's surface after the cleansing and annealing process. The surface appeared smoother after the cleansing process. After the annealing process, images of the grains could be seen. This was suspected to be a layer of mixed oxides, formed by the oxidation process of oxygen and the metal components in the stainless steel such as Ni, Cr and Fe. The mixed metal oxides can enhance the surface roughness and establish better chemical adhesion of the surface with the coating catalyst.

Figure 4 illustrates the morphologies of the coated surface after the wash-coat process. The thickness of catalyst was determined at 144 μm. The catalyst layer was seen as uniformly scattered and homogeneous along the channel. Figure 4(b2) demonstrates micro-sized particles with different distribution of macro-pore.

Figure 2. H_2-TPR profile of (**a**) pure NiO used as reference and (**b**) 40 wt% Ni-CeO$_2$/Cr$_2$O$_3$ catalyst calcined at 500 °C. Where α, β, and γ are weak, moderate and strong peak interaction temperature, respectively.
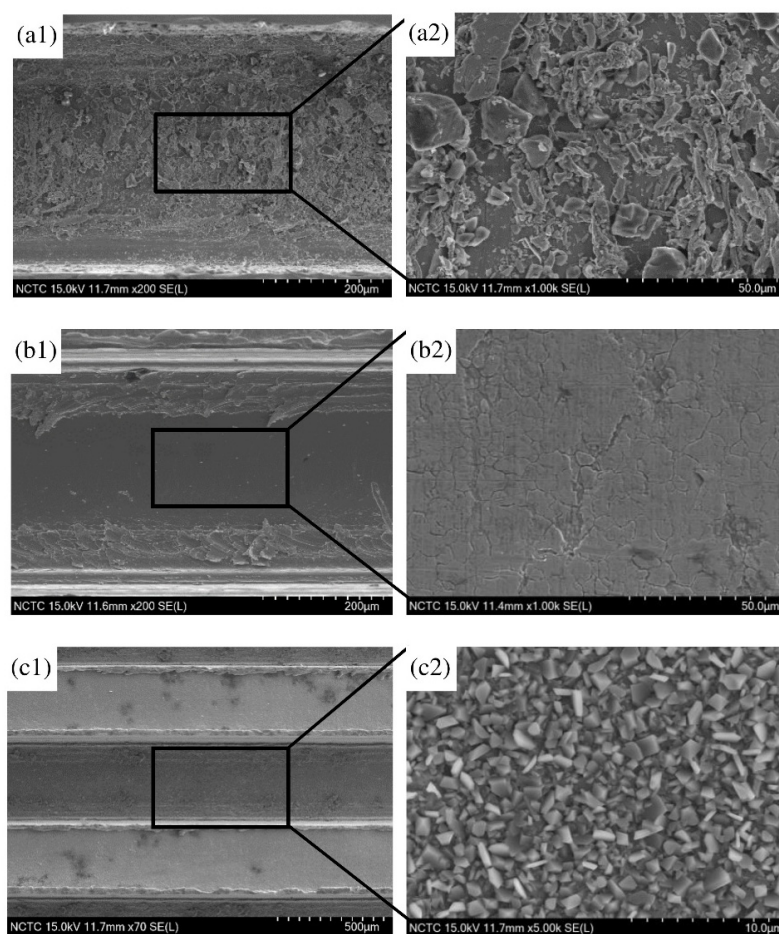
Figure 3. Photograph and surface morphology of the micro-channel plates: (**a1**) ×200 and (**a2**) ×1000 before cleansing; (**b1**) ×200 and (**b2**) ×1000 after cleansing, with 20% citric acid; (**c1**) ×70 and (**c2**) ×50,000 after annealing at 800 °C.
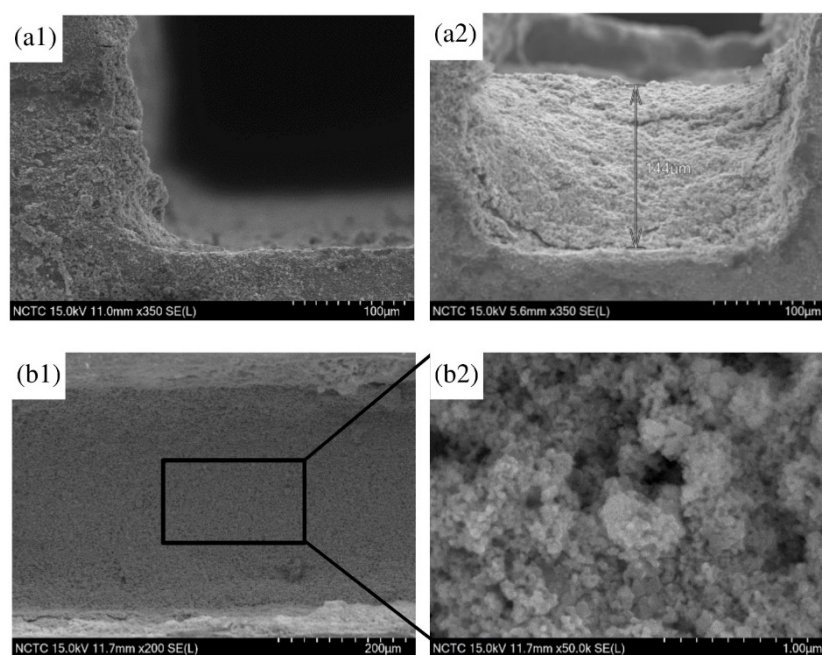
Figure 4. Photograph and surface morphology of the micro-channel plates coating with 40 wt% Ni-CeO$_2$/Cr$_2$O$_3$ catalyst: (**a1**) ×350 before coating, side view; (**a2**) ×350 after coating, side view; (**b1**) ×200 and (**b2**) ×50,000 after coating, top view.

### 2.1.4. FTIR Spectroscopy before and after Exposure to Reaction

FTIR spectroscopy was applied to identify the adsorbed functional species on the catalyst when being exposed in the gaseous reactant stream, CO$_2$ + H$_2$, at 270 °C. Figure 5 demonstrates the adsorbed species of the pre- (top) and post-exposure (bottom) catalyst. The deepest strong band at 3413–3421 cm^{-1} is ascribed to the O–H stretching vibration in OH groups, due to from adsorbed water and/or H-chemisorbed atom on metal. The bridged bidentate carbonate species was banded at 1630 cm^{-1}, 1320 cm^{-1}, and 1018 cm^{-1}, assigned to the asymmetric, symmetric CO$_3$-stretching, and OCO-bending (ν_{as}(CO$_3$), ν_s(CO$_3$), and δ(OCO), respectively, as a vibration mode), which appeared in both pre- and post-exposure catalysts. While the carbonate species of the fresh catalyst were likely to be the result of an uncompleted combustion process during the calcination (in static air at 500 °C for 12 h at 10 °C·min^{-1} of heating rate), those in the spent catalyst were suspected to indicate the CO$_2$ adsorption.

Importantly, the bands located at 1383 and 1470 cm^{-1}, which are assigned to the CH–bending and asymmetric CO$_2$-stretching (δ(CH) and ν_{as}(COO) as a vibration mode), are attributed to formate species, according to chelating bidentate.
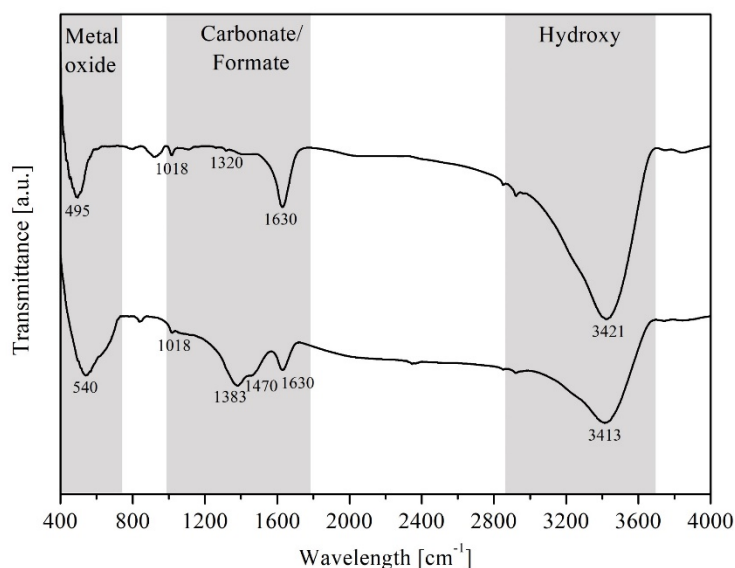
Figure 5. FTIR spectra of adsorbed gases on 40 wt% $NiO/Ce_{0.5}Cr_{0.5}O_2$ catalyst, where (top line) the fresh calcined catalyst and (below line) spent catalyst are under exposure to $CO_2 + H_2$ at 270 °C, both fresh and spent samples were pre-treated with hydrogen at 500 °C for 2 h and after cooling down to room temperature under Ar atmosphere.

In addition, the bending vibration of NiO bonding was indicated at a wavelength ranging from 495 to 540 cm^{-1} [27]. These results indicated that the carbonates and formates are the intermediates for the methanation via CO_2 hydrogenation. The mechanism of CO_2 hydrogenation in the presence of $Ni-CeO_2/Cr_2O_3$ is proposed as schematically shown below in Figure 6:
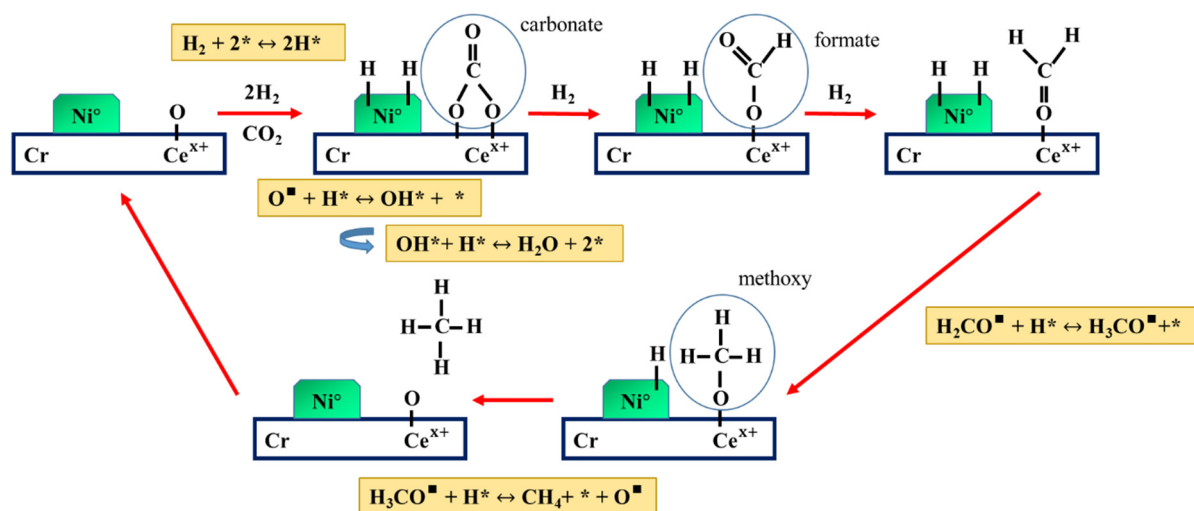
**Figure 6.** Mechanism proposed for CO_2 hydrogenation over the surface of $Ni-CeO_2/Cr_2O_3$.

2.2. Catalytic Activity of $NiO-Ce_{0.5}Cr_{0.5}O_2$ towards CO_2 Methanation

2.2.1. Effect of Molar Feed Ratio vs. Temperature

From Figure 7, it can be seen that CO_2 conversion was increased when the amount of hydrogen was increased (or ratio of H_2 to CO_2 was changed from 2:1 to 4:1) (Figure 7a), indicating that the CO_2 was excess in the first case (Figure 7a). CH_4 selectivity was found to increase when the percentage of H_2 in the feed reactant increased (Figure 7b), meaning that the H_2 is the limiting agent when the H_2 to CO_2 ratio was 2 to 1 (Figure 7a) (the

similar trend was observed by Abbelo et al. (2013) [28] and Rahmani et al. (2014)) [29], where the increasing ratio of H_2/CO_2 would cause an increase in CO_2 conversion, as the reaction was promoted by a high concentration of dissociated hydrogen on the catalyst surface [29–31]. The results agreed with work reported by Daroughegi et al. (2017) [30], which stated that the stoichiometric ratio of H_2/CO_2 should be equaled 4.0 due to the basicity property on the nickel's surface species. This means that four molecules of H_2 are required to suppress CO_2 adsorption on active of the catalyst since the H_2 molecule can be entirely adsorbed on the catalyst's surface, which simultaneously has much more hydrogenate on the carbonate species.

In addition, it can be seen that in the reverse water gas shift (RWGS) reaction, $(CO_2 + H_2 \leftrightarrow CO + H_2O)$ was more promoted at the lower ratio of H_2/CO_2, which resulted in a decrease in CH_4 selectivity. By temperature range, the conversions were found to increase during the operating temperature ranging from 250 to 310 °C. Decreases in conversions and product selectivity were due to the occurring of RWGS reaction which is thermodynamically favorable at a higher temperature. The optimal temperature was determined to be at 310 °C for both ratios, providing CO_2 conversion and CH_4 selectivity at 18.57% and 95.06% for (2:1 ratio) and at 73.75% and 100% for (4:1 ratio), respectively. This result agreed with the H_2-TPR result which reported peak α centered at 310 °C.
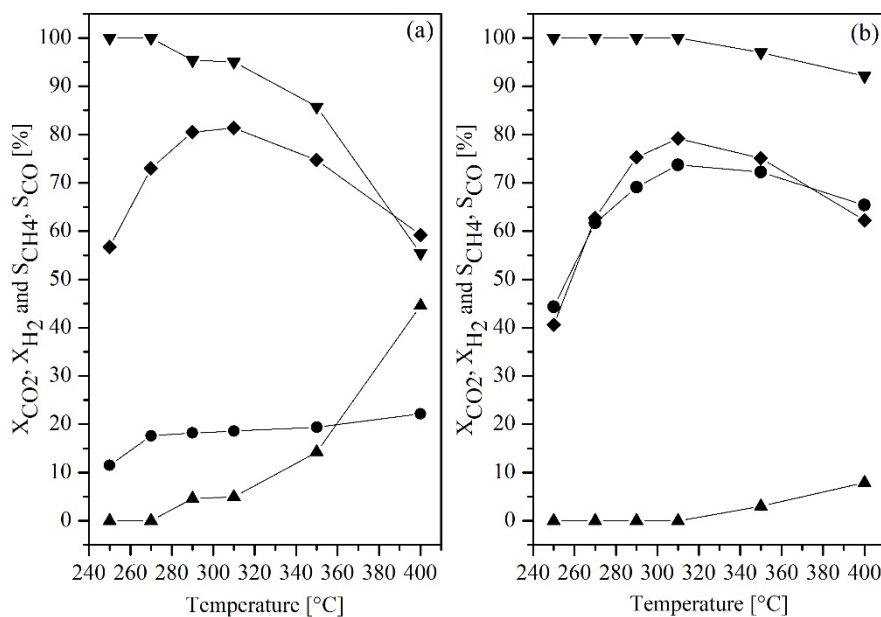
Figure 7. CO_2 (●), H_2 (◆) conversion and CH_4 (▼), CO (▲) selectivity over 40 wt% Ni-CeO_2/Cr_2O_3 catalyst as a function of temperature and various H_2/CO_2 molar ratio; (**a**) 2:1 and (**b**) 4:1 with WHSV = 56,500 $ml_N \cdot h^{-1} \cdot g^{-1}_{cat}$.

Table 1 compares catalytic performance of the catalyst from this work tested in a micro-channel reactor, with other recent catalysts developed tested in a packed-bed reactor by other researchers. The 40 wt% Ni-CeO_2/Cr_2O_3 catalyst in a micro-channel reactor was found to possess the best performance at a lower operating temperature, even at the higher WHSV.

Table 1. Catalysts comparison for CO_2 methanation reaction.

Catalyst	Condition	WHSV $(ml_N \cdot h^{-1} \cdot gcat^{-1})$	CO_2 Conv. (%)	CH_4 Sel. (%)	* T50 (%)
1.71% Mn-Ni/Al_2O_3 [31]	H_2:CO_2:N_2 = 36:9:5 $T_{opt.}$ = 400 °C Reactor type = Packed-bed	48,000	82	98	280
20% Ni/Al_2O_3 [32]	$T_{opt.}$ = 350 °C Reactor type = Packed-bed	9000	82	100	265
10% Ni/CeO_2-ZrO_2 [33]	$T_{opt.}$ = 300 °C Reactor type = Packed-bed	20,000	55	97	262
2% Ce-20% Ni/Al_2O_3 [29]	H_2:CO_2 = 3.5:1 $T_{opt.}$ = 350 °C Reactor type = Packed-bed	9000	80	100	240
15% Ni-2% CeO_2/Al_2O_3 [34]	H_2:CO_2 = 4:1 $T_{opt.}$ = 350 °C Reactor type = Packed-bed	15,000	85	99	280
20% Ni/H-Al_2O_3 [35]	H_2:CO_2:N_2 = 60:15:25 $T_{opt.}$ = 290 °C Reactor type = Packed-bed	9600	95	99	234
30% Ni-5%Fe-Al_2O_3 [36]	H_2:CO_2:N_2 = 4:1:1.7 $T_{opt.}$ = 220 °C Reactor type = Packed-bed	9600	59	58	-
30% Ni-5 wt% Fe/Al_2O_3 [37]	H_2:CO_2 = 3.5:1.0 $T_{opt.}$ = 350 °C Reactor type = Packed-bed	9000	71	99	240
0.3% K-78%Ni/Al_2O_3 [38]	H_2:CO_2:N_2 = 72:18:10 $T_{opt.}$ = 350 °C Reactor type = Packed-bed	75,000	83	99	285
10% La-20%Ni/Al_2O_3 [39]	H_2:CO_2 = 3.5:1 $T_{opt.}$ = 350 °C Reactor type = Packed-bed	9000	78	100	-
KCC-1 [40]	H_2:CO_2 = 4:1 $T_{opt.}$ = 450 °C Reactor type = Packed-bed	50,000	49	39	-
20% Ni-20%-CeO_2/MCM-41 [41]	H_2:CO_2 = 4:1 $T_{opt.}$ = 380 °C Reactor type = Packed-bed	9000	86	99	290
25% Ni/Al_2O_3 [30]	H_2:CO_2 = 3.5:1 $T_{opt.}$ = 350 °C Reactor type = Packed-bed	9000	74	99	300
10% Ni-0.5%Pd/Al_2O_3 [42]	H_2:CO_2:Ar = 4:1:8.5 $T_{opt.}$ = 250 °C Reactor type = Packed-bed	5800	91	97	227
10% Ni-3%Co/$Ce_{0.6}Zr_{0.4}O_2$ [13]	H_2:CO_2 = 4:1 $T_{opt.}$ = 300 °C Reactor type = Packed-bed	12,500	83	94	260
$La_{0.5}Ce_{0.5}NiO_3$/ZrO_2 [43]	H_2:CO_2:N_2 = 16:4:5 $T_{opt.}$ = 250 °C Reactor type = Packed-bed	15,000	76	100	230
40% Ni-CeO_2/Cr_2O_3 This work	H_2:CO_2 = 4:1 $T_{opt.}$ = 310 °C Reactor type = Microchannel	56,500	74	100	255

* T50 denoted that temperature at 50% CO_2 conversion.

2.2.2. Kinetic Measurement

The kinetic parameters of CO_2 methanation in the presence of 40 wt% Ni-CeO_2/Cr_2O_3 was studied in a micro-channel reactor at temperature ranging from 250 to 280 °C. The parameters calculation was performed using the POLYMATH 6.10 Software. The temperature range was selected based on the minimal side reactions and its initial reaction-controlled regime. The ratio of H_2 to CO_2 was varied at 1:1, 1:2, and 4:1. The power-law rate expression, as described in Equation (4), was applied to fit the rate of CO_2 methanation. A simple rate equation was considered due to the fact that the rate of the reaction changes with the change in concentration of each reactant, whereas the concentration changes on

the catalyst's surface was ignored. Therefore, the overall reaction rate for the irreversible reaction is focused only on the reactants:

$$- r_{CO_2} = -r_{H_2} = -\frac{d[CO_2]}{dt} = -\frac{d[H_2]}{dt} = k(T)[H_2]^n[CO_2]^m \tag{1}$$

where $-r_{CO_2}$ and $-r_{H_2}$ are the reaction rate in $mol \cdot L^{-1} \cdot s^{-1}$, $[CO_2]$ and $[H_2]$ in $mol \cdot L^{-1}$ are molar concentration of each species, k is the reaction rate constant with dependence on the temperature, n and m are the reaction order with respect to CO_2 and H_2.

The rate constant, which describes the temperature dependency of the reaction rate, is assumed to obey the Arrhenius relationship according the following equation:

$$\ln k(T) = -Ea(1000/RT) + \ln k_0 \tag{2}$$

The negative apparent activation energy (E_{app}), achieved from the Arrhenius plots as illustrated in Figure 8, was determined at $4.85\ kJ \cdot mol^{-1}$. The orders of the reaction with respect to H_2 and CO_2 were estimated at 0.33 to 1.07 for n^{th}-order and 0.40 to 0.53 for m^{th}-order. The apparent activation energy was benchmarked with other previous works as shown in Table 2.
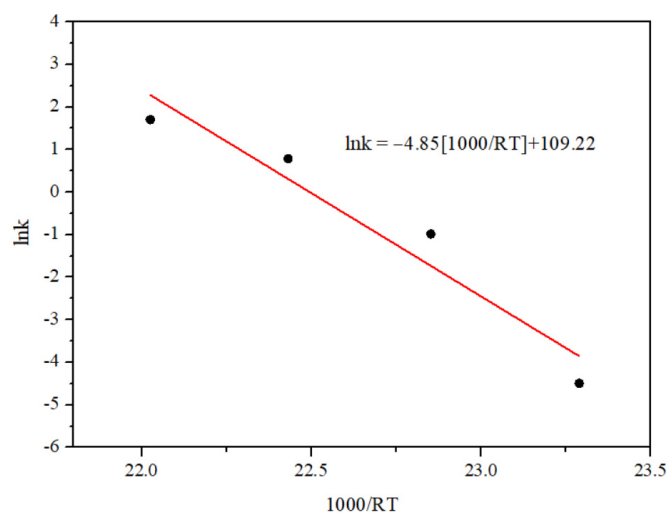
Figure 8. Arrhenius plot for estimated kinetic parameters for CO_2 methanation on 40 wt% Ni-CeO_2/Cr_2O_3 catalyst.

Table 2. Summary of activation energy from previous reported study.

Catalyst	Condition	Temperature Range (°C)	Ea (kJ/mol)	Ref.
10% Ni/ZSM-5	$H_2:CO_2 = 4:1$ GHSV = 2400 h^{-1} P = 1 bar Reactor type = Packed-bed	200–450	52.69	[44]
18% Ni/Al_2O_3	$H_2:CO_2:N_2 = 72:18:10$ GHSV = 8000–12,000 h^{-1} = 10 bar Reactor type = Packed-bed	250–280	120.4	[45]
42% NiO/Al_2O_3	$H_2:CO_2 = 3:7, 5:5, 3:7$ F = 100 $ml_N \cdot min^{-1}$ P = 1 bar Reactor type = Packed-bed	210–315	80–90	[46]

Table 2. *Cont.*

| Catalyst	Condition	Temperature Range (°C)	Ea (kJ/mol)	Ref.
NiAl(O)$_x$	H$_2$:CO$_2$:Ar = 4:1:20 WHSV = 2400 l$_N$·h^{-1}·g^{-1}$_{cat}$ P = 3–9 bar Reactor type = Packed-bed	250–340	82.1–84.7	[47]
12% Ni/Al$_2$O$_3$	H$_2$:CO$_2$:Ar = 150:50:6 F = 206 ml$_N$·min^{-1} P = 20 bar Reactor type = Packed-bed	170–210	92	[48]
10% Ru/Al$_2$O$_3$	H$_2$:CO$_2$:He = 4:1:20 GHSV = 90,000–262,920 h^{-1} P = 1 bar Reactor type = Packed-bed	230–245	66.1	[49]
40% Ni-CeO$_2$/Cr$_2$O$_3$	H$_2$:CO$_2$ = 1:1, 1:2, and 4:1 F = 60 ml$_N$·min^{-1} P = 1 bar Reactor type = Microchannel	250–280	4.85	This work

3. Methodology

3.1. Pre-Treatment of Micro-Channel Reactor

A micro-channel reactor was fabricated from two micro-structured stainless steel (316 L) plates, laser welded together by the Thai German Institute (TGI) (Chonburi, Thailand). Each plate accommodated 14 channels with dimensions of 25 mm in length, 0.37 mm in width, and 0.30 μm in depth. The gaseous inlet was assumed to be uniformly distributed amongst the 14 slots by 3 physical dots, locating at the corners of an isosceles triangle. The steps of micro-channel pre- and post-treatment was prepared as illustrated in Figure 9, where (a) is the specimens before cleansing, (b) is after cleansing with citric acid, and (c) is after annealing at 800 °C. During the cleansing process, the plates were cleaned by immersing in citric acid (20% by volume) in an ultrasonic bath for 5 h (step 1) before being rinsed by deionized water (step 2). In order to generate grains of mixed oxides on the surface, the micro-channel plates were then annealed at 800 °C for 10 h with 1 °C·min^{-1} of heating rate risen from room temperature (step 3). Finally, the two plates were laser-welded together after completing the catalyst coating process, described in the next section.

3.2. Catalyst Coating on the Micro-Channeled Substrates

3.2.1. Catalyst Powder Preparation

Ni-CeO$_2$/Cr$_2$O$_3$ was synthesized using the one-pot hydrolysis method described elsewhere [20]. The percentage of Ni was 40% by weight with a ratio of CeO$_2$ to Cr$_2$O$_3$ at 1 to 1. The stoichiometric amount of the relevant nitrate precursors: (Ni(NO$_3$)$_2$.6H$_2$O (CARLO ERBA, ≥99.0%); Ce(NO$_3$)$_3$·6H$_2$O (ALDRICH, ≥99.0%); Cr(NO$_3$)$_2$·6H$_2$O (ACROS, ≥99.0%): were dissolved together in 100 mL demineralized water. The mixture was then heated to 80 °C while stirred continuously. Ammonium carbonate (NH$_4$)$_2$CO$_3$ solution (1 M) was added the drop-wise into the previous mixture to maintain the solution pH at 8.8 to 9.0, while the mixed solution was heated to 120 °C, to evaporate water. The residual was afterwards calcined in static air at 500 °C for 12 h at 10 °C·min^{-1} heating rate. The resulting catalyst powder was ground and sieved to achieve the particle size of 35 μm or smaller.
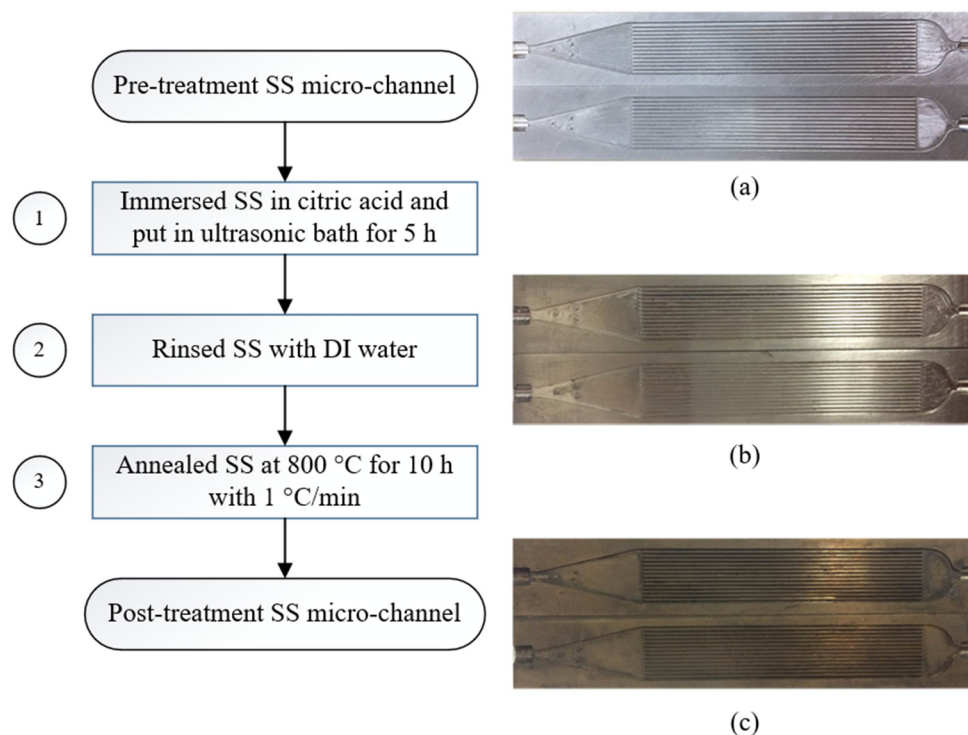
Figure 9. Steps of micro-channel pre- and post-treatment preparation: (**a**) before cleansing, (**b**) after cleansing with citric acid, and (**c**) after annealing at 800 °C.

### 3.2.2. Catalyst Suspended Solution Preparation

This method was adapted from a procedure previously described elsewhere [50]. The mass ratio of Ni-CeO$_2$/Cr$_2$O$_3$:H$_2$O:PVA:CH$_3$COOH was fixed at 10:84:5:1 in this study. Polyvinyl alcohol (PVA) solution, as a binder, was prepared beforehand by dissolving in deionized water under vigorous stirring at 65 °C for 2 h before being left overnight without stirring. The sieved catalyst was dispersed into the binder solution under a vigorous stirring condition. Acetic acid (CH$_3$COOH, 17 M) was added into the solution while being heated to reach the temperature of 65 °C where it remained for 2 h. After the well-mixed solution was naturally cooled down to room temperature, the stirring was continued for 3 days.

3.2.3. Wash-Coat

The prepared catalyst suspension was wash-coated onto the surface of the micro-structured substrates. The plates were left at room temperature for 4 h before they were dried in an oven at 120 °C overnight. The excess polymer binder was eliminated by a calcination process at 500 °C for 3 h. Approximately 32 mg of the catalyst were successfully coated on the surface of each plate after two times of coating.

3.2.4. Micro-Channel Reactor Fabrication

Two of the coated plates were laser-weld together. Figure 10 illustrates the configuration of the micro-channel reactor. The adhesion between the catalyst and surface of the substrates were tested using a drop test [20]. Both ends of the micro-channel reactor were connected with 1/8-inch stainless steel tubes by welding. To ensure there was no leakage, the following was performed: (i) one end of the reactor was clogged with a plug, (ii) inert gas was compressed through the reactor at 5 bar, (iii) the reactor was immersed into water, and (iv) a leakage can be regarded if air bubbles are noticed.
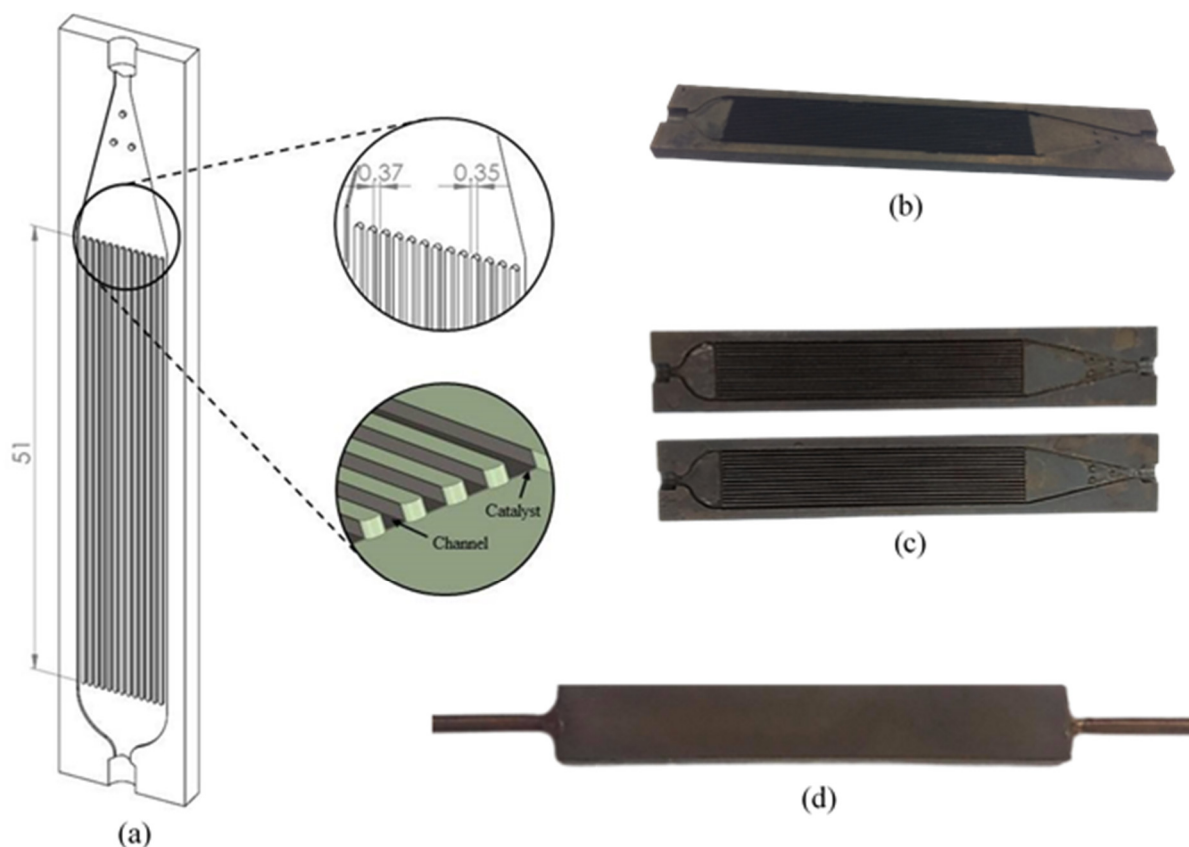
Figure 10. Two plates of micro-channeled stainless steel 316 L; (**a**) drawing scale, (**b**) after wash coating, (**c**) after burning binder at 500 °C, and (**d**) reactor assembling by laser welding.

4. Characterizations

An X-ray diffractometer (Bruker AXS, Berlin, Germany, Diffractometer D8 equipment using CuKα (λ = 1.5418 Å) as a radiation source at 40 kV and 30 mA with a scanning speed of $0.02°$ s^{-1} in 2θ ranges from 20° to 70° was used to identify the phase structure of the prepared catalyst. The Joint Committee on Powder Diffraction Standards (JCPDSs) cards were referenced with the result. The in situ H_2 temperature-programmed reduction (H_2-TPR) technique was applied to investigate the reducibility of the catalyst. For this test, 0.5 g of the catalyst was charged into the quartz tube reactor (i.d. = 10 mm) before being pre-treated in 100 $ml_N \cdot min^{-1}$ of 10 vol% O_2/Ar at 700 °C for 1 h, in order to eliminate any possible impurities on the catalyst surface. After it cooled down to room temperature, 5 vol% of H_2/Ar was introduced into the packed-bed reactor at 100 $ml_N \cdot min^{-1}$ while the temperature was risen at 5 °C.min^{-1} from room temperature to 950 °C. H_2 consumption was monitored by a real-time quadrupole mass spectrometer (MS, Omnistar GSD 320, Pfeiffer Vacuum, Asslar, Germany) in the SEM-MID mode. The surface morphology of the material's surface was examined using a scanning electron microscope (SEM, SU-8230 Hitachi, Hitachi High-Tech, Minato-ku Tokyo, Japan) with an accelerating voltage of 15 kV. The sample was immobilized by mounting onto a metal stud with double sided carbon tape then gold coated to improve conductivity. The in situ Fourier-transform infrared spectroscopy (FTIR Perkin Elmer, Spectrum 2000 spectrometer, Perkin Elmer, Massachusetts, United States) equipped with a wavenumber resolution of 1 cm^{-1} in the range between 400 and 4000 cm^{-1} was applied to define the adsorbed species on the surface of 40 wt% Ni-CeO_2/Cr_2O_3 during CO_2 + H_2 exposure at 270 °C.

5. Catalytic Reaction on a Micro Channel Stainless Reactor

The experiments were carried out in the lab-prepared micro channel reactor under atmospheric pressure. The weight of the catalyst coated onto the reactor was measured at 63.7 mg. The coated catalyst was firstly in situ activated at 500 °C (testified by H_2-TPR) in pure H_2 (99.995%, BIG) flowing through the system at 100 $ml_N.min^{-1}$ for 2 h, before being cooled down to the selected operating temperature, which varied at 250, 270, 290, 310, 350, to 400 °C. Ar was then purged through the catalyst bed to remove any possible excess H_2 and unwanted physisorption. A flow of the mixed gaseous reactant, H_2 and CO_2, at each selected ratio of 2:1 and 4:1, was switched into the reactor at 60 $ml_N·min^{-1}$ of the total flow rate, giving 56,500 $ml_N·h^{-1}·g^{-1}_{cat}$ of WSHV. The effluent gas stream was automatically sampled every 7 min and analyzed online through GC-TCD chromatography (Shimadzu GC-2014ATF). The CO_2 conversion (X_{CO2}) and CH_4 selectivity (S_{CH4}) were calculated using the below equations:

$$CO_2 \text{ conversion}, X_{CO_2}[\%] = \left(\frac{F_{CO_2}^{in} - F_{CO_2}^{out}}{F_{CO_2}^{in}} \right) \times 100 \qquad (3)$$

$$CH_4 \text{ selectivity}, S_{CH_4}[\%] = \left(\frac{F_{CH_4}}{F_{CH_4} + F_{CO}} \right) \times 100 \qquad (4)$$

where $F_{CO_2}^{in}$ and $F_{CO_2}^{out}$ represent the volume flow rate of CO_2 in the feed stream and outlet stream, F_{CH_4} and F_{CO} denote the volume flow rate of product gas stream.

6. Conclusions

A total of 40 wt% of nickel-based catalyst on $Ce_{0.5}Cr_{0.5}O_2$ support was synthesized using the one-pot hydrolysis method. The best operating condition was experimented and estimated to be showing the best catalytic performance at the operating temperature of 310 °C, WHSV of 56,500 $ml_N·h^{-1}·g^{-1}_{cat}$, and feed ratio of H_2 to CO_2 at 4 to 1. The influence of the variation parameter on the catalytic activity CO_2 methanation was explained by the kinetics and the operatory conditions. The mechanistic of CO_2 methanation reaction was comprehensively revealed by FTIR spectroscopy, the main mechanism over the 40 wt% $NiO/Ce_{0.5}Cr_{0.5}O_2$ catalyst did not require CO but the reaction intermediates were replaced by carbonates and formates. The elementary reaction pathway occurred through hydrogenation on carbonates species, while formates species continued to form, and further, methoxy species. This mechanism implied that the CO_2 adsorption was occupied on a strong bonding of nickel oxide active site (on $Ce_{0.5}Cr_{0.5}O_2$ support) (testified by H_2-TPR). The activation energy of such a catalyst for CO_2 methanation in a micro-channel reactor was calculated at 4.85 kJ/mol, which was much (10 to 30 times) lower than other catalysts tested in packed-bed reactors.

Author Contributions: Conceptualization, V.T.; methodology, V.T.; software, Y.A.-l.; validation, Y.A.-l. and C.W.; formal analysis, C.K.; investigation, N.S.-N.; resources, N.L.; data curation, V.T.; writing—original draft preparation, V.T.; writing—review and editing, U.W.H.; visualization, N.L.; supervision, U.W.H.; project administration, N.L.; funding acquisition, U.W.H. All authors have read and agreed to the published version of the manuscript.

Conflicts of Interest: The authors declare no conflict of interest.

References

1. Engelbrecht, N.; Everson, R.C.; Bessarabov, D.; Kolb, G. Microchannel reactor heat-exchangers: A review of design strategies for the effective thermal coupling of gas phase reactions. *Chem. Eng. Process. Process Intensif.* **2020**, *157*, 108164. [CrossRef]
2. Takoudis, C.G. The catalytic synthesis of hydrocarbons from H_2/CO mixtures over the group VIII metals: Comments on methanation kinetics. *J. Catal.* **1982**, *78*, 265. [CrossRef]
3. Ye, R.-P.; Liao, L.; Reina, T.R.; Liu, J.; Chevella, D.; Jin, Y.; Fan, M.; Liu, J. Engineering Ni/SiO_2 catalysts for enhanced CO_2 methanation. *Fuel* **2021**, *285*, 119151. [CrossRef]
4. Atzori, L.; Rombi, E.; Meloni, D.; Monaci, R.; Sini, M.F.; Cutrufello, M.G. Nanostructured Ni/CeO_2–ZrO_2 Catalysts for CO_2 Conversion into Synthetic Natural Gas. *J. Nanosci. Nanotechnol.* **2019**, *19*, 3269–3276. [CrossRef]
5. Gac, W.; Zawadzki, W.; Rotko, M.; Greluk, M.; Słowik, G.; Kolb, G. Effects of support composition on the performance of nickel catalysts in CO_2 methanation reaction. *Catal. Today* **2020**, *357*, 468–482. [CrossRef]
6. Bukhari, S.; Chong, C.; Setiabudi, H.; Ainirazali, N.; Ab Aziz, M.A.; Jalil, A.; Chin, S. Optimal Ni loading towards efficient CH_4 production from H_2 and CO_2 over Ni supported onto fibrous SBA-15. *Int. J. Hydrogen Energy* **2019**, *44*, 7228–7240. [CrossRef]
7. Jaffar, M.M.; Nahil, M.A.; Williams, P.T. Parametric Study of CO_2 Methanation for Synthetic Natural Gas Production. *Energy Technol.* **2019**, *7*, 1–12. [CrossRef]
8. Cárdenas-Arenas, A.; Cortés, H.S.; Bailón-García, E.; Davó-Quiñonero, A.; Lozano-Castelló, D.; Bueno-López, A. Active, selective and stable $NiO-CeO_2$ nanoparticles for CO_2 methanation. *Fuel Process. Technol.* **2021**, *212*, 106637. [CrossRef]
9. Riani, P.; Valsamakis, I.; Cavattoni, T.; Escribano, V.S.; Busca, G.; Garbarino, G. Ni/SiO_2-Al_2O_3 catalysts for CO_2 methanation: Effect of La_2O_3 addition. *Appl. Catal. B Environ.* **2021**, *284*, 119697. [CrossRef]
10. Daroughegi, R.; Meshkani, F.; Rezaei, M. Enhanced low-temperature activity of CO_2 methanation over ceria-promoted $Ni-Al_2O_3$ nanocatalyst. *Chem. Eng. Sci.* **2021**, *230*, 116194. [CrossRef]
11. Karam, L.; Bacariza, M.C.; Lopes, J.M.; Henriques, C.; Massiani, P.; El Hassan, N. Assessing the potential of $xNi-yMg-Al_2O_3$ catalysts prepared by EISA-one-pot synthesis towards CO_2 methanation: An overall study. *Int. J. Hydrogen Energy* **2020**, *45*, 28626–28639. [CrossRef]
12. Shen, W.-J.; Okumura, M.; Matsumura, Y.; Haruta, M. The influence of the support on the activity and selectivity of Pd in CO hydrogenation. *Appl. Catal. A Gen.* **2001**, *213*, 225–232. [CrossRef]
13. Pastor-Pérez, L.; Saché, E.; Jones, C.; Gu, S.; Arellano-Garcia, H.; Reina, T. Synthetic natural gas production from CO_2 over $Ni-x/CeO_2$-ZrO_2 (x = Fe, Co) catalysts: Influence of promoters and space velocity. *Catal. Today* **2018**, *317*, 108–113. [CrossRef]
14. Wang, F.; He, S.; Chen, H.; Wang, B.; Zheng, L.; Wei, M.; Evans, D.G.; Duan, X. Active Site Dependent Reaction Mechanism over Ru/CeO_2 Catalyst toward CO_2 Methanation. *J. Am. Chem. Soc.* **2016**, *138*, 6298–6305. [CrossRef]
15. Pan, Q.; Peng, J.; Sun, T.; Gao, D.; Wang, S.; Wang, S. CO_2 methanation on $Ni/Ce_{0.5}Zr_{0.5}O_2$ catalysts for the production of synthetic natural gas. *Fuel Process. Technol.* **2014**, *123*, 166–171. [CrossRef]
16. Shannon, R.D. Revised effective ionic radii and systematic studies of interatomic distances in halides and chalcogenides. *Acta Crystallogr. A* **1976**, *32*, 751–767. [CrossRef]
17. Fu, Z.; Yu, Y.; Li, Z.; Han, D.; Wang, S.; Xiao, M.; Meng, Y. Surface Reduced CeO2 Nanowires for Direct Conversion of CO_2 and Methanol to Dimethyl Carbonate: Catalytic Performance and Role of Oxygen Vacancy. *Catalysts* **2018**, *8*, 164. [CrossRef]
18. Singh, P.; Hegde, M.S.; Gopalakrishnan, J. $Ce_{2/3}Cr_{1/3}O_{2+y}$: A New Oxygen Storage Material Based on the Fluorite Structure. *Chem. Mater.* **2008**, *20*, 7268–7273. [CrossRef]
19. Singh, P.; Hegde, M.S. $Ce_{0.67}Cr_{0.33}O_{2.11}$: A New Low-Temperature O_2 Evolution Material and H_2 Generation Catalyst by Thermochemical Splitting of Water. *Chem. Mater.* **2010**, *22*, 762–768. [CrossRef]
20. Nie, W.; Zou, X.; Chen, C.; Wang, X.; Ding, W.; Lu, X. Methanation of Carbon Dioxide over Ni–Ce–Zr Oxides Prepared by One-Pot Hydrolysis of Metal Nitrates with Ammonium Carbonate. *Catalysts* **2017**, *7*, 104. [CrossRef]
21. Wongsartsai, C.; Tongnan, V.; Sornchamni, T.; Siri-Nguan, N.; Laosiripojana, N.; Hartley, M.; Hartley, U.W. CO_2 utilization via methanation using 40% $Ni/Ce_xCr_{1-x}O_2$ as a novel catalyst: A comparative study of packed-bed and micro-channel reactors. *React. Kinet. Mech. Catal.* **2020**, *131*, 1–17. [CrossRef]
22. Sobukawa, H. Development of Ceria-Zirconia Solid Solutions and Future Trends. *R D Rev. Toyota CRDL* **2002**, *37*, 1–5.
23. Yang, P.; Yang, S.; Shi, Z.; Meng, Z.; Zhou, R. Deep oxidation of chlorinated VOCs over CeO_2 -based transition metal mixed oxide catalysts. *Appl. Catal. B Environ.* **2015**, *162*, 227–235. [CrossRef]
24. Cai, M.; Wen, J.; Chu, W.; Cheng, X.; Li, Z. Methanation of carbon dioxide on Ni/ZrO_2-Al_2O_3 catalysts: Effects of ZrO_2 promoter and preparation method of novel ZrO_2-Al_2O_3 carrier. *J. Nat. Gas Chem.* **2011**, *20*, 318–324. [CrossRef]
25. Zhu, Z.-Q.; Cheng, X.-D.; Ye, W.-P.; Min, J. Synthesis of $NiCr_2O_4$ spinel coatings with high emissivity by plasma spraying. *Int. J. Miner. Met. Mater.* **2012**, *19*, 266–270. [CrossRef]
26. Jayaram, V.; Preetam, S.; Reddy, K.P.J. Experimental Investigation of Nano Ceramic Material Interaction with High Enthalpy Argon under Shock Dynamic Loading. *Appl. Mech. Mater.* **2011**, *83*, 66–72. [CrossRef]
27. Mochizuki, S. Infrared Spectra of NiO Microcrystals at High Temperatures. *Phys. Status Solidi* **1982**, *110*, 219–225. [CrossRef]
28. Abelló, S.; Berrueco, C.; Montane, D. High-loaded nickel–alumina catalyst for direct CO_2 hydrogenation into synthetic natural gas (SNG). *Fuel* **2013**, *113*, 598–609. [CrossRef]
29. Rahmani, S.; Rezaei, M.; Meshkani, F. Preparation of promoted nickel catalysts supported on mesoporous nanocrystalline gamma alumina for carbon dioxide methanation reaction. *J. Ind. Eng. Chem.* **2014**, *20*, 4176–4182. [CrossRef]

30. Daroughegi, R.; Meshkani, F.; Rezaei, M. Enhanced activity of CO_2 methanation over mesoporous nanocrystalline Ni–Al_2O_3 catalysts prepared by ultrasound-assisted co-precipitation method. *Int. J. Hydrogen Energy* **2017**, *42*, 15115–15125. [CrossRef]
31. Zhao, K.; Li, Z.; Bian, L. CO_2 methanation and co-methanation of CO and CO_2 over Mn-promoted Ni/Al_2O_3 catalysts. *Front. Chem. Sci. Eng.* **2016**, *10*, 273–280. [CrossRef]
32. Sepehri, S.; Rezaei, M. Preparation of Highly Active Nickel Catalysts Supported on Mesoporous Nanocrystalline γ-Al_2O_3 for Methane Autothermal Reforming. *Chem. Eng. Technol.* **2015**, *38*, 1637–1645. [CrossRef]
33. Ashok, J.; Ang, M.; Kawi, S. Enhanced activity of CO_2 methanation over Ni/CeO_2-ZrO_2 catalysts: Influence of preparation methods. *Catal. Today* **2017**, *281*, 304–311. [CrossRef]
34. Liu, H.; Zou, X.; Wang, X.; Lu, X.; Ding, W. Effect of CeO_2 addition on Ni/Al_2O_3 catalysts for methanation of carbon dioxide with hydrogen. *J. Nat. Gas Chem.* **2012**, *21*, 703–707. [CrossRef]
35. He, S.; Li, C.; Chen, H.; Su, D.; Zhang, B.; Cao, X.; Wang, B.; Wei, M.; Evans, D.G.; Duan, X. A Surface Defect-Promoted Ni Nanocatalyst with Simultaneously Enhanced Activity and Stability. *Chem. Mater.* **2013**, *25*, 1040–1046. [CrossRef]
36. Hwang, S.; Hong, U.G.; Lee, J.; Gil Seo, J.; Baik, J.H.; Koh, D.J.; Lim, H.; Song, I.K. Methanation of carbon dioxide over mesoporous Ni–Fe–Al_2O_3 catalysts prepared by a coprecipitation method: Effect of precipitation agent. *J. Ind. Eng. Chem.* **2013**, *19*, 2016–2021. [CrossRef]
37. Moghaddam, S.V.; Rezaei, M.; Meshkani, F.; Daroughegi, R. Carbon dioxide methanation over Ni-M/Al_2O_3 (M: Fe, CO, Zr, La and Cu) catalysts synthesized using the one-pot sol-gel synthesis method. *Int. J. Hydrogen Energy* **2018**, *43*, 16522–16533. [CrossRef]
38. He, L.; Lin, Q.; Liu, Y.; Huang, Y. Unique catalysis of Ni-Al hydrotalcite derived catalyst in CO_2 methanation: Cooperative effect between Ni nanoparticles and a basic support. *J. Energy Chem.* **2014**, *23*, 587–592. [CrossRef]
39. Rahmani, S.; Rezaei, M. A Comparative Study on the Kinetics of Carbon Dioxide Methanation over Bimetallic and Monometallic Catalysts. *Iran J. Hydrog. Fuel Cell* **2016**, *1*, 59–71. [CrossRef]
40. Hamid, M.; Firmansyah, M.L.; Triwahyono, S.; Jalil, A.; Mukti, R.; Febriyanti, E.; Suendo, V.; Setiabudi, H.D.; Mohamed, M.; Nabgan, W. Oxygen vacancy-rich mesoporous silica KCC-1 for CO_2 methanation. *Appl. Catal. A Gen.* **2017**, *532*, 86–94. [CrossRef]
41. Wang, X.; Zhu, L.; Liu, Y.; Wang, S. CO_2 methanation on the catalyst of Ni/MCM-41 promoted with CeO_2. *Sci. Total Environ.* **2018**, *625*, 686–695. [CrossRef]
42. Mihet, M.; Lazar, M.D. Methanation of CO_2 on Ni/γ-Al_2O_3: Influence of Pt, Pd or Rh promotion. *Catal. Today* **2018**, *306*, 294–299. [CrossRef]
43. Li, S.; Liu, G.; Zhang, S.; An, K.; Ma, Z.; Wang, L.; Liu, Y. Cerium-modified Ni-La_2O_3/ZrO_2 for CO_2 methanation. *J. Energy Chem.* **2020**, *43*, 155–164. [CrossRef]
44. Guo, X.; Traitangwong, A.; Hu, M.; Zuo, C.; Meeyoo, V.; Peng, Z.; Li, C. Carbon Dioxide Methanation over Nickel-Based Catalysts Supported on Various Mesoporous Material. *Energy Fuels* **2018**, *32*, 3681–3689. [CrossRef]
45. Türks, D.; Mena, H.; Armbruster, U.; Martin, A. Methanation of CO_2 on Ni/Al_2O_3 in a Structured Fixed-Bed Reactor—A Scale-Up Study. *Catalysts* **2017**, *7*, 152. [CrossRef]
46. Maatman, R.; Sjouke, H. A kinetic study of the methanation of CO_2 over nickel-alumina. *J. Catal.* **1980**, *62*, 349–356. [CrossRef]
47. Koschany, F.; Schlereth, D.; Hinrichsen, O. On the kinetics of the methanation of carbon dioxide on coprecipitated NiAl(O). *Appl. Catal. B Environ.* **2016**, *181*, 504–516. [CrossRef]
48. Hubble, R.A.; Lim, J.Y.; Dennis, J.S. Kinetic Studies of CO_2 Methanation over a Ni/γ-Al_2O_3 Catalyst. *Faraday Discuss.* **2016**, *192*, 529–544. [CrossRef] [PubMed]
49. Duyar, M.; Ramachandran, A.; Wang, C.; Farrauto, R.J. Kinetics of CO_2 methanation over Ru/γ-Al_2O_3 and implications for renewable energy storage applications. *J. CO_2 Util.* **2015**, *12*, 27–33. [CrossRef]
50. Ngoenthong, N.; Hartley, M.; Sornchamni, T.; Siri-Nguan, N.; Laosiripojana, N. Comparison of Packed-Bed and Micro-Channel Reactors for Hydrogen Production via Thermochemical Cycles of Water Splitting in the Presence of Ceria-Based Catalysts. *Processes* **2019**, *7*, 767. [CrossRef]